Sensitivity Analysis of Virtual Synchronous Generator-Based Grid-Forming Inverters under Low Short-Circuit Ratio and Low System Inertia

Janith Wijesingha, Lasantha Meegahapola, Xinghuo Yu
School of Engineering, RMIT University, Melbourne, Australia

***Abstract*—As conventional synchronous generators are progressively replaced by inverter-based resources (IBRs), the resulting reduction in system inertia leads to new stability challenges. This paper aims to evaluate the dynamic performance of a virtual synchronous generator (VSG)–based grid-forming inverters (GFMIs) under low short circuit ratio (SCR) and low-inertia conditions. Although several network characteristics, such as the X/R ratio and SCR, have been widely studied, the combined influence of low SCR and system inertia, with the focus on current-limiting strategies during severe faults, remains significantly underexplored. Therefore, virtual impedance (VI) and direct current-limiting schemes are evaluated for VSG- and power synchronization control (PSC)-based GFMIs for comparison. The results show that system inertia and SCR strongly influence fault ride-through capability and post-fault stability, and the choice of current-limiting strategy plays a critical role beyond over-current protection. Further analysis of control-parameter variations indicates that stability can be improved even under worst-case scenarios through appropriate parameter adjustment, highlighting the need for robust GFMI designs for operation in such low-strength networks.**

***Index Terms*—Direct current limiter, grid forming inverter (GFMI), short circuit ratio (SCR), system inertia, virtual impedance (VI), virtual synchronous generator (VSG).**

I. Introduction

The transition of power networks has been towards replacing conventional synchronous generators (SGs) with inverter-based resources (IBRs) such as solar PV, wind, and fuel cells. At present, most IBRs are grid-interfaced through grid-following inverters (GFLIs) [1]. With advances in control concepts, GFLIs not only track the maximum power point but also provide grid-supportive functions, including fault ride-through (FRT) capabilities. However, since GFLIs rely on a phase-locked loop (PLL) to follow the grid voltage phasor, they can lose synchronism and become unstable under weak-grid conditions [2]. To address this limitation, the grid-forming inverter (GFMI) concept has emerged, enabling inverters to establish and regulate their own voltage phasor [3]. Among various GFMI types, the virtual synchronous generator (VSG) configuration closely mimics the dynamic behavior of a conventional synchronous generator [4].

The evaluation of VSG performance varies significantly depending on the active and reactive power control strategies. For example, in [5], the synchronverter approach is introduced, while [6] proposed the ISE-Lab control topology to emulate the swing dynamics of a synchronous machine using virtual inertia and damping. Furthermore, [4] discusses power synchronization control (PSC) methods that incorporate decoupling mechanisms to mitigate cross-coupling between the dq components. As various types of GFMIs, particularly VSG concepts, continue to emerge, evaluating their performance has become increasingly important. Accordingly, the performance of various VSG control strategies has been extensively analyzed under diverse operating scenarios, including different load conditions, varying X/R ratios, varying short-circuit ratios (SCRs), and network faults [4], [7].

In power systems, inertia refers to the ability of the system to resist changes in frequency, commonly expressed as the rate of change of frequency (RoCoF). This concept can be discussed in two aspects: system inertia and inverter virtual inertia. Here, inverter virtual inertia is a tuning parameter, while system inertia refers to the aggregate inertia of all synchronous generators connected to the grid [8]. In real-world applications of GFMI, the interaction between GFMI control dynamics and system inertia may be critical. Another important factor of performance analysis is the SCR measured at the point of common coupling (PCC) of the inverter, which relates to the strength of the grid. Moreover, current control limiter methods also have an impact on stability against severe disturbances. The most applicable current limiter methods are virtual impedance (VI) [9], direct current limiter [10], and voltage limiter [11]. The design of the VI-based current limiter requires a tradeoff between stability requirements and dynamic response. Among them, the direct current limiter constrains the current-reference magnitude to a constant value when activated. Moreover, the phase can be flexibly adjusted with improved versions (”priority-based”), and the stability can be further enhanced by changing the power reference change during current-limiter activation. Therefore, the consideration of the current limiter plays a major role under the given system conditions.

This work evaluates the performance of the VSG-based GFMI under high and low system inertia and weak grid conditions and compares it with other PSC-based strategies to assess its dynamic stability. In particular, the study investigates the impact of the current limiter strategy against the aforementioned conditions. Furthermore, the effects of two key control parameters of virtual inertia and virtual damping are also examined to determine their impact on the worst-case scenario.

II. Control Principles of the VSG-based GFMI

This study employs the VSG-based GFMI model (ISE-Lab model) proposed in [6] as a benchmark, and this section

979-8-3315-8138-1

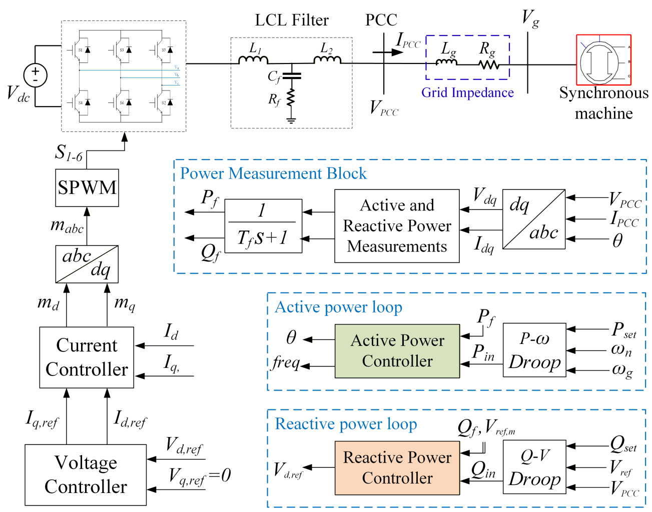

Fig. 1: Overview of cascaded control architecture of GFMI.

presents the detailed modeling of GFMI secondary control layers and current limiting strategies.

A. System Representation

In order to observe the transient behavior of the system, an electromagnetic transient (EMT)-based MATLAB/Simulink model is developed as shown in Fig. 1. In most of the studies, grid-connected GFMI is represented by connecting it to an infinite bus. However, an infinite bus does not replicate the system inertia that exists in a practical power network. Therefore, the proposed study connects the VSG-based GFMI to a synchronous generator, enabling the system inertia to be varied easily. Accordingly, the simplified synchronous machine block implements the mechanical system that can be described as,

$$\omega_g = \frac{1}{2Hs + K_d}\left[T_m - T_e\right] + \frac{\omega_n}{s} \tag{1}$$

Here, H denotes the inertia constant, and K_d is the damping coefficient, which is maintained at a fixed value in this study. Since the purpose of the synchronous generator model is to replicate high- and low-inertia conditions corresponding to different levels of IBR penetration, keeping K_d at a constant value ensures that changes in system response are solely attributed to variations in system inertia. Moreover, T_m and T_e represent the mechanical and electrical torque, respectively, while ω_n denotes the nominal angular frequency. Typically, in high-inertia systems, the value of H is maintained around 8-10 s, whereas with increased penetration of IBRs, it may drop below 2 s. Therefore, the range of H is selected as 1-10 s in this study to replicate both low- and high-inertia system conditions.

B. Modeling of VSG- based GFMI

The inverter is connected to the grid via a LCL filter as shown in Fig. 1(a). The selection of the filter parameters follows the procedure discussed in [12]. In the VSG-based GFMI controller, the active power–frequency loop regulates system frequency through virtual inertia and damping, and the reactive power–voltage loop maintains terminal voltage

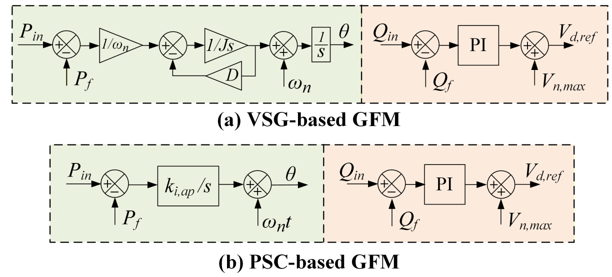

Fig. 2: Active and reactive power control (APC and RPC) architecture of (a) VSG-based GFMI and (b) PSC-based GFMI.

stability. Accordingly, the active power control of the VSG-based GFMI can be expressed in the Laplace domain as follows.

$$\omega = \left(\left[P_{in} - P_f\right]\frac{1}{\omega_n} - D\Delta\omega\right)\frac{1}{Js} + \omega_n \tag{2}$$

Here, ω denotes the inverter angular frequency, and ω_n represents the nominal frequency, which is considered constant. Moreover, $P_{in} = P_{set} + (\omega_n - \omega_g)D_p$, where P_{set} and P_f are the active power setpoint and the measured active power, respectively. To enable droop-based control, the grid angular frequency, ω_g must be measured at the PCC, which can be obtained using a PLL.

Moreover, the reactive power control of the VSG-based GFMI model can be defined as,

$$V_{d,ref} = \left(k_{pq} + \frac{k_{iq}}{s}\right)\left[Q_{in} - Q_f\right] + V_{n,max} \tag{3}$$

Here, $V_{d,ref}$ denotes the d-axis voltage reference that feeds into the voltage controller. Furthermore, $Q_{in} = Q_{set} + (V_n - E)D_q$, where Q_{set} and Q_f represent the reactive power setpoint and the measured reactive power, respectively. Moreover, $V_n = V_{rated}/\sqrt{3}$ is the nominal voltage and $V_{n,max} = \sqrt{2}V_n$ denotes the maximum nominal voltage limit. The block diagram of active and reactive power control (APC and RPC) of VSG-based GFMI is illustrated in Fig. 2(a). To enable a fair performance comparison with the VSG-based GFMI, a PSC-based GFMI architecture is also considered in this study. The main distinction between the two architectures lies in the control action of the APC, as illustrated in Fig. 2(b).

C. Considered current limiting strategies

In order to enable the fault ride-through capability, a current limiter is essential to protect the inverter from over-current stress during faults or transient disturbances. The commonly used current limiting methods are as follows.

(a) Virtual impedance (VI): Virtual impedance is commonly used for current limiting in GFMI due to its fast response. However, its effectiveness depends on precise tuning, as higher virtual inductance may cause instability at fault clearance [13]. Therefore, a VI-based current limiter is developed as follows [9].

$$\begin{bmatrix} V^*_{d,ref} \\ V^*_{q,ref} \end{bmatrix} = \begin{bmatrix} V_{d,ref} \\ V_{q,ref} \end{bmatrix} - \begin{bmatrix} R_{vir} & -X_{vir} \\ X_{vir} & R_{vir} \end{bmatrix}\begin{bmatrix} I_d \\ I_q \end{bmatrix} \tag{4}$$

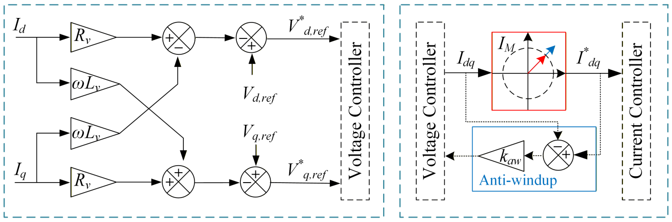

(a) (b)

Fig. 3: The block diagrams of (a) virtual impedance and (b) direct current limiter.

Here, $V^*_{d,ref}$ and $V^*_{q,ref}$ are new voltage references derived from the VI-based current limiter as shown in Fig. 3(a). The virtual resistance (R_{vir}) and reactance (X_{vir}) can be defined as [14],

$$X_{vir} = \begin{cases} R_{vir} = 0, & I_R \leq I_{th} \\ \lambda_{XR} R_{vir}, \text{s.t. } R_{vir} = \beta\left(I_R - I_{th}\right), & I_R > I_{th} \end{cases} \tag{5}$$

In (5), λ_{XR}, I_R and I_{th} are X/R ratio of the grid impedance, the RMS current at PCC, and the threshold value (1.5 p.u.) of the current. Moreover, β is a constant parameter selected to ensure the desired current limitation under the worst-case fault condition, such as a three-phase bolted fault.

(b) Direct current limiter: This method is implemented before the inner current controller, effectively limiting the fault current magnitude. Moreover, unlike virtual-impedance-based current limiting, this approach requires anti-windup mechanisms in the voltage control loop to prevent integrator windup, as illustrated in Fig. 3(b). The direct current limiter is developed as follows [10].

$$I^*_{dq} = \begin{cases} I_{dq}, & |I_{dq}| \leq I_{th} \\ \dfrac{I_{th}}{|I_{dq}|} I_{dq}, & |I_{dq}| > I_{th} \end{cases} \tag{6}$$

III. Performance Analysis Under Low SCR and Varying System Inertia Environment

This section analyzes the impact of system strength under low SCR conditions for different current-control strategies. For comparison, a PSC-based GFMI is also considered, employing the same current-control methods described in Section II-C.

A. Parameter Tuning Validation

Fig. 4 validates the parameter tuning of the VSG-based GFMI (with VI-based current limiter) under a wide range of grid strengths and system inertia levels. For both weak-grid ($SCR = 1.5$) and stronger-grid ($SCR = 5$) conditions, the GFMI maintains stable and well-damped active power, reactive power, and frequency responses for different inertia constants, demonstrating robust performance against variations in system strength. More specifically,, the frequency remains within the permissible operating band of 0.98–1.02 p.u. during and immediately after the high-impedance three-phase fault (not severe), and the corresponding RoCoF is maintained within 1 Hz/s, in compliance with Australian frequency operation standards. Note that qualitatively similar variations are observed with the direct current-limiting strategy. Based on these observations, the controller parameters are tuned to satisfy both stability and grid-code requirements and are subsequently used in the following case study. The selected GFMI parameters are summarized in Table I.

TABLE I: Key System Parameters

Symbol	Description	Values
	Grid parameters	
V_g	L-L RMS voltage	400 V
f_g	Grid frequency	50 Hz
H	System inertia constant	1-10 s
SCR	Short circuit ratio	1.5-5
X/R	X/R ratio	8.5
	Inverter parameters	
P_{rated}	Rated power	20 kW
V_{dc}	DC link voltage	600 V
L_{f_1}	Inverter side filter inductance	2.5 mF
L_{f_2}	Grid side filter inductance	1.5 mF
C_f	Filter capacitance	60 μF
R_f	Filter damping resistor	1.3 Ω
	GFMI control layer parameters	
$k_{p,cc}, k_{i,cc}$	Current controller PI gains	88, 1253
$k_{p,vc}, k_{i,vc}$	Voltage controller PI gains	0.8, 10
D_p	$P-\omega$ droop coefficient	1×10^4 rad/W.s
D_q	$Q-V$ droop coefficient	1×10^3 V/VAr
D	Damping coefficient (VSG)	23 Ws/rad
J	Inertia coefficient (VSG)	0.8 Ws^2/rad
$k_{p,rp}, k_{i,rp}$	RPC PI gains (VSG, PSC)	0.01, 0.2
$k_{i,ap}$	APC integral gains (PSC)	0.001

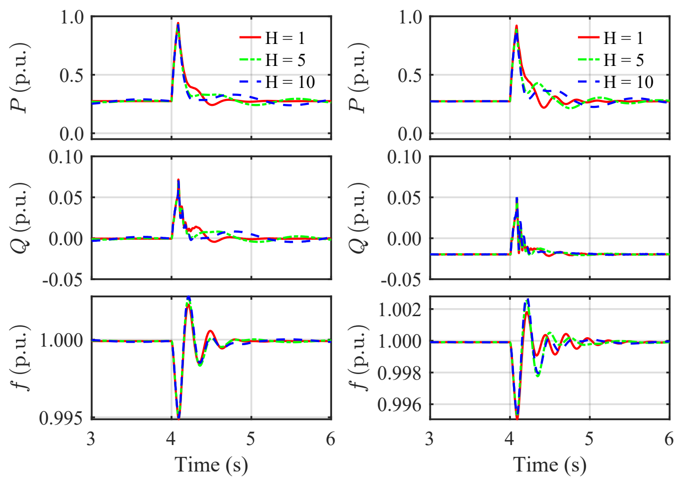

(a) (b)

Fig. 4: Parameter-tuning validation of the VSG-based GFMI under (a) SCR $= 1.5$ and (b) SCR $= 5$ conditions, for varying inertia constants, subjected to a high-impedance three-phase fault at $t = 4$ s and cleared after 80 ms.

B. Case Study: Performance Comparison Against Sever Low Impedance Fault

In this case study, a severe fault is introduced to evaluate the dynamic performance of different grid-forming (GFM) strategies with current-limiting schemes under weak-grid conditions and varying inertia levels, as illustrated in Fig. 5. To compare post-disturbance performance, an oscillation-recovery-based

979-8-3315-8138-1

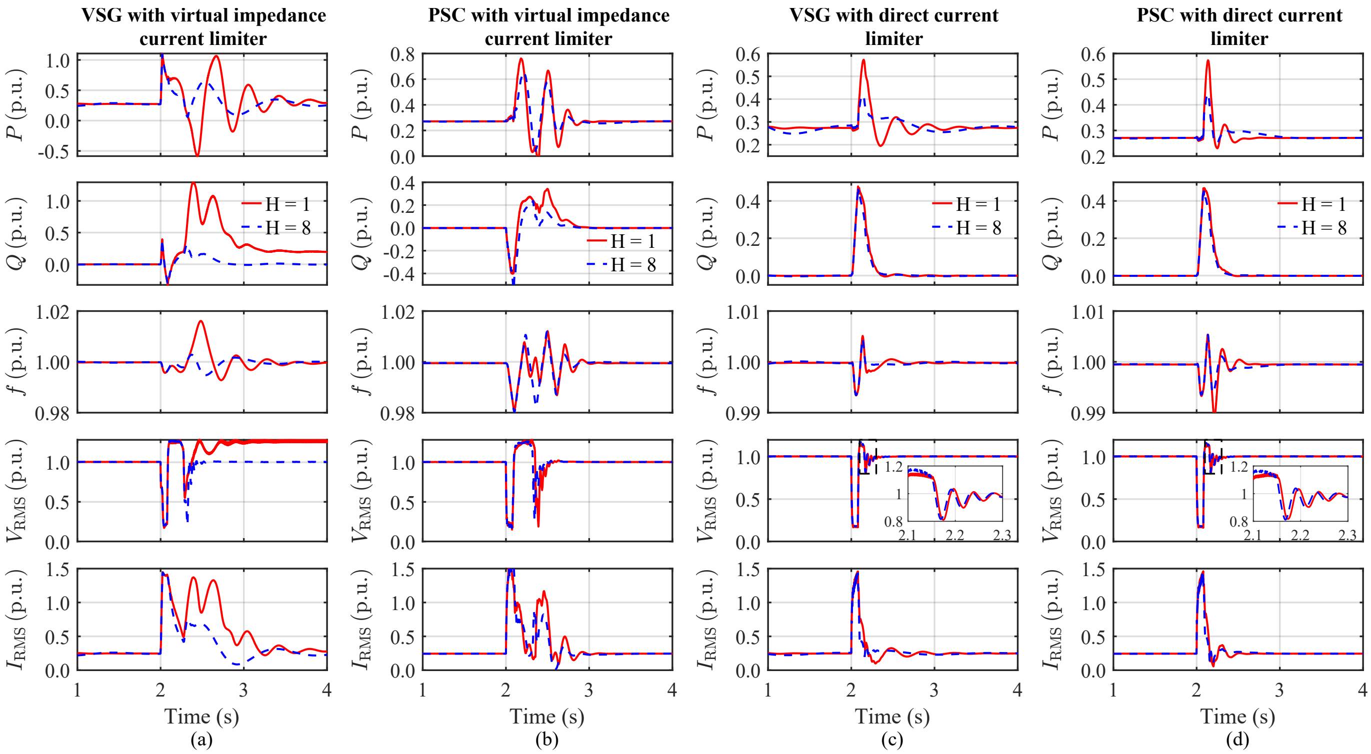

Fig. 5: Comparison of adaptive virtual impedance and direct current-limiting strategies for grid-forming converters with VSG- and PSC-based control, under weak-grid condition (SCR $= 1.5$) and varying system inertia constants $H = 1$ and $H = 8$, subjected to a severe three-phase fault at $t = 2$ s, with fault clearance after 80 ms.

TABLE II: Comparison of GFMI strategies with current limiting under low-SCR conditions for high- and low-inertia systems.

	System Inertia (s)	Robustness Metric (ζ)	
		Active Power	Reactive Power
VSG + VI current limiter	$H = 1$	0.138	unstable
	$H = 8$	**0.257**	**0.104**
PSC + VI current limiter	$H = 1$	0.033	0.038
	$H = 8$	**0.036**	**0.078**
VSG + Direct current limiter	$H = 1$	0.286	0.557
	$H = 8$	**0.367**	**0.700**
PSC + Direct current limiter	$H = 1$	0.261	0.699
	$H = 8$	**0.270**	**0.699**

robustness metric (ζ) is introduced. The lower values of ζ are considered as lower the robustness and vice versa.

$$\zeta = \frac{1}{\sqrt{1 + \left(\frac{2\pi}{ln\left(\frac{Y_0}{Y_1}\right)}\right)^2}} \tag{7}$$

Here, Y_0 and Y_1 correspond to two adjacent positive peak amplitudes of post-disturbance oscillation. Accordingly, ζ for the active and reactive power responses is reported in Table II.

Under the VI current-limiting strategy, the VSG-based GFMI with low inertia ($H = 1$) experiences a collapse of the voltage control loop following the severe fault, indicating insufficient damping and limited robustness under weak-grid conditions (refer Fig. 5(a)). In contrast, the PSC-based GFMI with VI current limiter depicted in Fig. 5(b) exhibits pronounced active-power oscillations, which translate into higher RoCoF and consequently result in a reduced ζ as in the Table. II. Despite this degradation at low inertia, both the VSG- and PSC-based GFMI with VI current limiter demonstrates improved dynamic performance when operating with higher inertia, highlighting the higher inertial energy smooths the interaction between the VI and the grid-forming voltage control loop. When the direct current-limiting strategy is employed, both VSG- and PSC-based GFMIs maintain stable operation across the considered inertia levels. As observed in Fig. 5(c) and Fig. 5(d), and robustness metrics summarized in Table II. However, higher system inertia leads to reduced overshoot and enhanced stability compared to lower inertia cases under direct current limiting, leading to fast frequency recovery. This behavior indicates that, unlike the VI-based approach, the direct limiter mitigates adverse inertia-dependent interactions during post-fault recovery.

According to the RMS current responses shown in Fig. 5, both current-limiting strategies effectively constrain the inverter current within the specified over-current limit of 1.5 p.u. Beyond providing over-current protection, the current-limiting strategy strongly influences the post-fault dynamic response of the inverter. However, it is evident that system stability degrades under low-inertia conditions, and this behavior can be further exacerbated by more severe faults or longer fault durations.

979-8-3315-8138-1

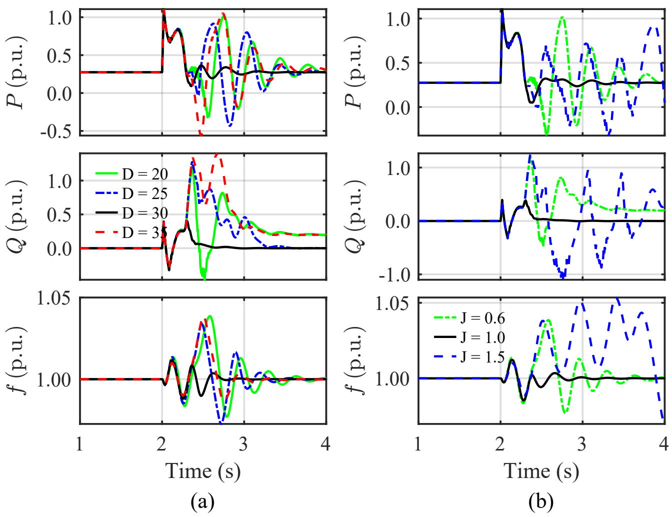

Fig. 6: Dynamic response of the VSG-based GFMI under with $H = 1$ and $SCR = 1.5$ conditions, considering a VI-based current limiter under (a) varying virtual damping (D) and (b) varying inertia constant (J), subjected to a severe fault.

C. Impact of Damping Constant and Virtual Inertia on Low-SCR and Low-Inertia Systems

This section analyzes the impact of virtual damping (D) and virtual inertia (J) constant under $SCR = 1.5$ and $H = 1$ s condition, which shows instability in the case study (Section III.B).

According to Fig. 6(a), increasing the virtual damping coefficient to $D = 30$ significantly improves the dynamic performance by effectively suppressing oscillations and ensuring convergence to the steady state. This indicates that the damping coefficient primarily governs how rapidly oscillations are attenuated. However, excessive damping introduces additional phase lag in the frequency control loop, which leads to low-frequency oscillations, as observed for $D = 35$ in Fig. 6(a). Next, the impact of J is examined while keeping the $D = 23$. As shown in Fig. 6(b), increasing J to 1.0 improves the overall dynamic response. From (2), a small J results in a high integral gain in the APC, causing rapid frequency and phase-angle variations that strongly couple with the voltage and RPC, potentially leading to instability. Increasing J reduces this integral gain and slows the frequency dynamics, thereby mitigating the instability of the system. Therefore, J determines how strongly and how fast the inverter frequency responds to disturbances. However, excessive J makes the power–frequency loop overly sluggish, and the GFMI cannot adjust frequency fast enough to track power balance, leading to higher oscillations. Therefore, under low inertia and low SCR, the system is more sensitive to controller parameters. This emphasizes the requirement for a robust control concept to retain performance under such conditions.

IV. Conclusion and Future Work

This study investigated the dynamic behavior of VSG-based GFMIs operating under low-inertia and low short-circuit-ratio conditions. The roles of VI and direct current-limiting strategies were also examined and compared with a PSC-based GFMI. The results demonstrate that both system inertia and SCR have a significant impact on the transient fault ride-through performance and post-fault stability of grid-forming inverters. Under low SCR and low inertia, the VSG-based GFMI with a VI current limiter showed instability during severe voltage disturbances, demonstrating the strong influence of the current-limiting strategy on system performance. The analysis further indicates that stability can still be achieved under such conditions through retuning of the internal control parameters. However, maintaining stability across a wide range of SCR and inertia values remains practically challenging. Therefore, future work will focus on developing robust control strategies to ensure stable operation of grid-forming controllers under variations in external system parameters, such as system inertia, SCR, X/R ratio, and uncertainties, such as the effects of multi-inverter interactions.

References

[1] J. Wijesingha, L. Meegahapola, and X. Yu, "Enhancing the dynamic performance of grid following inverters in distribution networks using integral terminal sliding mode control," *IEEE Trans. Power Syst.*, 2025.

[2] Y. Li, Y. Gu, and T. C. Green, "Revisiting grid-forming and grid-following inverters: A duality theory," *IEEE Trans. Power Syst.*, vol. 37, no. 6, pp. 4541–4554, 2022.

[3] D. B. Rathnayake, M. Akrami, C. Phurailatpam, S. P. Me, S. Hadavi, G. Jayasinghe, S. Zabihi, and B. Bahrani, "Grid forming inverter modeling, control, and applications," *Ieee Access*, vol. 9, pp. 114 781–114 807, 2021.

[4] C. Liyanage, I. Nutkani, L. Meegahapola, and M. Jalili, "Stability enhancement of power synchronisation control based grid-forming inverter under varying network characteristics," *IEEE Trans. Sustain. Energy*, vol. 15, no. 3, pp. 1799–1813, 2024.

[5] Q.-C. Zhong and G. Weiss, "Synchronverters: Inverters that mimic synchronous generators," *IEEE Trans. Ind. Electron.*, vol. 58, no. 4, pp. 1259–1267, 2010.

[6] T. Shintai, Y. Miura, and T. Ise, "Oscillation damping of a distributed generator using a virtual synchronous generator," *IEEE Trans. Power Del.*, vol. 29, no. 2, pp. 668–676, 2014.

[7] N. Mohammed, H. Udawatte, W. Zhou, D. J. Hill, and B. Bahrani, "Grid-forming inverters: A comparative study of different control strategies in frequency and time domains," *IEEE Open J. Ind. Electron. Soc.*, vol. 5, pp. 185–214, 2024.

[8] Australian Energy Market Operator (AEMO), "Inertia in the nem explained," Australian Energy Market Operator, Tech. Rep., 2023, accessed: 21 October 2025. [Online]. Available: https://www.aemo.com.au/-/media/files/initiatives/engineering-framework/2023/inertia-in-the-nem-explained.pdf

[9] A. Ordono, A. Sanchez-Ruiz, M. Zubiaga, F. J. Asensio, and J. A. Cortajarena, "Current limiting strategies for grid forming inverters under low voltage ride through," *Renewable and Sustainable Energy Reviews*, vol. 202, p. 114657, 2024.

[10] B. Fan and X. Wang, "Equivalent circuit model of grid-forming converters with circular current limiter for transient stability analysis," *IEEE Trans. Power Syst.*, vol. 37, no. 4, pp. 3141–3144, 2022.

[11] J. Chen, F. Prystupczuk, and T. O'Donnell, "Use of voltage limits for current limitations in grid-forming converters," *CSEE Journal of Power and Energy Systems*, vol. 6, no. 2, pp. 259–269, 2020.

[12] J. Wijesingha, L. Meegahapola, and X. Yu, "Performance analysis of active/reactive power control of a grid following voltage source inverter using sliding mode control," in *2024 IEEE 34th Australasian Universities Power Engineering Conference (AUPEC)*, pp. 1–6. IEEE, 2024.

[13] C. Luo, Y. Chen, Y. Xu, Z. Wang, S. Liao, Z. Xie, and Q. Li, "Two-stage transient control for vsg considering fault current limitation and transient angle stability," *IEEE Trans. Ind. Electron.*, vol. 71, no. 7, pp. 7169–7179, 2023.

[14] A. D. Paquette and D. M. Divan, "Virtual impedance current limiting for inverters in microgrids with synchronous generators," *IEEE Trans. Ind. Appl.*, vol. 51, no. 2, pp. 1630–1638, 2014.

979-8-3315-8138-1